Available online at www.sciencedirect.com
SCIENCE DIRECT®
Journal of Power Sources 117 (2003) 160–169
JOURNAL OF POWER SOURCES
www.elsevier.com/locate/jpowsour

Capacity fade study of lithium-ion batteries cycled at high discharge rates

Gang Ning, Bala Haran, Branko N. Popov*
Department of Chemical Engineering, University of South Carolina, Columbia, SC 29208, USA

Received 12 December 2002; accepted 20 December 2002

Abstract

Capacity fade of Sony US 18650 Li-ion batteries cycled using different discharge rates was studied at ambient temperature. The capacity losses were estimated after 300 cycles at 2*C* and 3*C* discharge rates and were found to be 13.2 and 16.9% of the initial capacity, respectively. At 1*C* discharge rate the capacity lost was only 9.5%. The cell cycled at high discharge rate (3*C*) showed the largest internal resistance increase of 27.7% relative to the resistance of the fresh cells. The rate capability losses were proportional with the increase of discharge rates. Half-cell study and material and charge balances were used to quantify the capacity fade due to the losses of primary active material (Li^+), the secondary active material ($LiCoO_2$/C)) and rate capability losses. It was found that carbon with 10.6% capacity loss after 300 cycles dominates the capacity fade of the whole cell at high discharge rates (3*C*). A mechanism is proposed which explains the capacity fade at high discharge rates.

Keywords: Lithium-ion batteries; Capacity fade; High discharge rates; Solid electrolyte interface (SEI)

1. Introduction

It is generally thought that lithium deposition, electrolyte decomposition, active material dissolution, phase transition inside the insertion electrode materials, and further passive film formation on the electrode and current collectors can affect up to different degrees the capacity fade of lithium-ion batteries [1–5]. Quantifying these degradation processes will not only help to improve the predictive capability of battery models but also help to elucidate the mechanism of capacity fade.

In this paper, capacity fade of Sony US 18650 lithium-ion batteries cycled using 1*C*, 2*C* and 3*C* discharge rates (up to 300 times) at ambient temperature was quantitatively measured. Parameters obtained through fitting EIS spectra and the SEM images taken for the carbon material samples were used to identify the primary cause of the capacity fade of the whole lithium-ion battery.

2. Experimental

Experiments were done on the Sony US 18650 (1.4 Ah) lithium-ion batteries. The batteries were charged under constant current and constant voltage protocol (CC–CV). The cells were initially charged under 1 A constant current until the voltage reached 4.2 V. Next, the voltage was kept constant at 4.2 V until the charge current decayed to 50 mA. To study the effects of the discharge rate, the cells were discharged at 1*C* (1.4 A), 2*C* (2.8 A) and 3*C* (4.2 A) rate. Cycling studies were done on Arbin Battery Test System. Data logging was set up on the basis of differential time and differential voltage during the process of charge or discharge by a computer with Mitspro software. Solartron SI 1255 HF Frequency Response Analyzer and Potentiostat/Galvanostat Model 273A were used for electrochemical characterization of these cells. For the studies of the capacity fade of whole-cells, cycling would be stopped every 50 cycles so that the batteries would be fully charged (with 1.0 A constant current and 4.2 V constant voltage) and then discharged at constant current (0.7 A) between the voltage windows from 4.2 to 2.5 V. The maximum cycle number in our studies was 300.

Internal dc resistance of the whole-cell was determined by intermittently interrupting the discharge current for 5 s in the process of discharge and the dc resistance of the whole-cell was calculated using the relationship: R_{dc} = (discharge voltage − open circuit voltage (0.1 s after the pulse rest))/discharge current (1 A).

In order to identify the cause of the capacity fade of the whole-battery, half-cell studies were carried out on both fresh and cycled batteries. Cells under fully discharged state

* Corresponding author. Tel.: +1-803-777-7314; fax: +1-803-777-8265.
E-mail address: popov@engr.sc.edu (B.N. Popov).

0378-7753/03/$ – see front matter © 2003 Elsevier Science B.V. All rights reserved.
doi:10.1016/S0378-7753(03)00029-6

(discharged to cut-off 2.5 V using (*C*/10) discharge rate) were cut open in a glove box filled with pure argon (National Gas and Welder-Class: Regular). Both the $LiCoO_2$ and carbon electrodes that were spirally wound together with the separator in between them were carefully taken out. Subsequently the material was cleaned and allowed to dry at ambient temperature for 1 h. Small pellets with a diameter of 1.1 cm were punched out of the electrode materials using a sharp steel punch. Since both sides of the current collectors were coated with active materials, the material on one side was scraped to ensure good contact with the steel current collectors of the T-shaped polypropylene Swagelock-type cells. Pellets prepared as mentioned above are the standard samples for all the experiments of the half-cell studies. In the T-shaped cells, pure lithium foil was used as both counter and reference electrodes. Separators were prepared through scissoring the separators in the commercial cells to the size of the pellet. Electrolyte used was 1 M $LiPF_6$ in a 1:1 mixture of ethylene carbonate (EC) and dimethyl carbonate (DMC).

T-cells/half-cells were charged or discharged with 150 μA to check the capacity. The voltage window is from 4.2 to 2.5 V for the $LiCoO_2$ half-cell while it is from 2.5 to 0.025 V for the carbon half-cell. EIS measurements were done on the whole-cells cycled up to 300 cycles under both fully charged state and fully discharged state. The batteries were held at least 1 h before impedance measurements in order to ensure the stability of the baseline voltage during such a test and in most cases this voltage fluctuation was less than 1 mV. The ac signal for the whole-cell study is a 10 mV sinusoidal voltage covering a frequency range from 1000 to 0.005 Hz. For half-cell impedance studies, different state-of-charge (SOC) was determined by controlling the charge time. The time interval between the Galvanostatic step and EIS measurement is fixed at 60 min. The frequency ranges from 100 kHz to 1 mHz.

3. Results and discussions

3.1. Charge and discharge study of whole battery

Fig. 1 shows the capacity fade of batteries as a function of cycle number. In order to compare performance of cells cycled at different rates, the capacity was checked with a 1 A discharge rate every 50 cycles. If discharge rate has no effect on cell capacity, all batteries should have the similar capacity at any cycle number. However, that is not the case in our studies. As can be seen, immediately after the first 50 cycles, capacity fade for batteries cycled at 1, 2 or 3*C* shows no big difference. But with cycling, capacity fade diverges. The battery cycled at 3*C* discharge rate loses almost 16.9% of its initial discharge capacity while the battery cycled at 1*C* and 2*C* discharge rates, loses 9.5 and 13.2% of its initial capacity after 300 cycles. Further, it is shown from the slope between 200 and 300 cycles that the rate of capacity fade is faster for 2 or 3*C*-discharge-rate-cycled batteries than for 1*C*-discharge-rate-cycled battery. These results indicate the discharge rate plays a strong role in determining the rate of capacity fade of Li-ion cells.

Fig. 2 shows the discharge capacity of batteries corresponding to their actual discharge rates and not to those normalized to 1 A discharge rate. In the case of the 1*C*-discharge-rate-cycled battery, capacity fades almost linearly with cycling. However, in case of 2 or 3*C*-discharge-rate-cycled batteries, discharge capacity drops quickly in the first

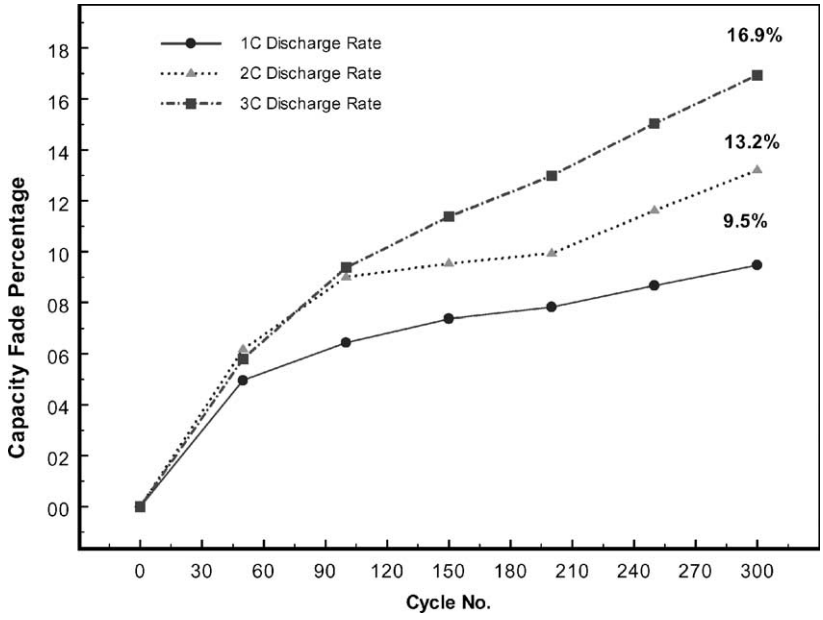

Fig. 1. Capacity fade of Sony US 18650 batteries under different discharge rates. The discharge capacity was checked at the same discharge rate (1 A constant current) once every 50 cycles.

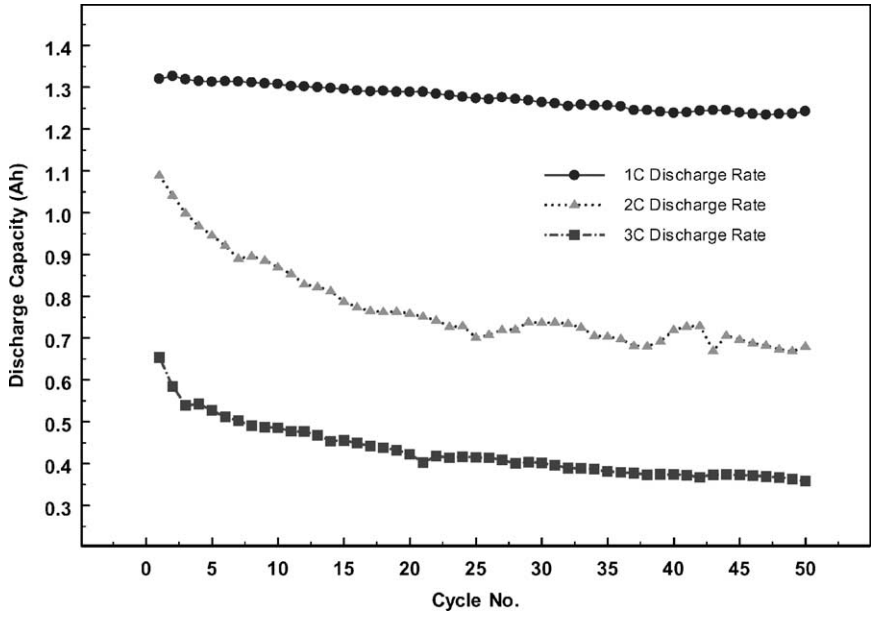

Fig. 2. Discharge capacity of Sony US 18650 batteries as a function of cycle number. The discharge capacity corresponds to its actual discharge rate (1, 2 or 3*C* discharge rates).

few cycles and then decreases linearly as it does in the case of 1*C* rate. After 50 cycles, the battery cycled at 1*C* discharge rate loses only 5% of its initial capacity (corresponding to 1*C* discharge rate) while batteries cycled at 2*C* and 3*C* lose 38 and 45% (corresponding to 2*C* and 3*C* discharge rate, respectively) of their initial capacity. Although the different discharge rates affect the capacity obtained, the fast drop in capacity in the first few cycles for the battery cycled at high discharge rates indicates that the internal resistance of these cells is large.

Fig. 3 shows the discharge profile of different cells that had been cycled up to 300 times. The discharge current was 0.7 A. Although the basic shape of these plots remained very similar to each other, we can still see that the voltage plateau of the battery cycled at the high discharge rate (2 or 3*C*) is shorter compared with that cycled at the low discharge rate (1*C*). The output voltage of the cell under constant current can be simply represented by Ohm's law as

$$V = E_0 - I \times R_T \quad (1)$$

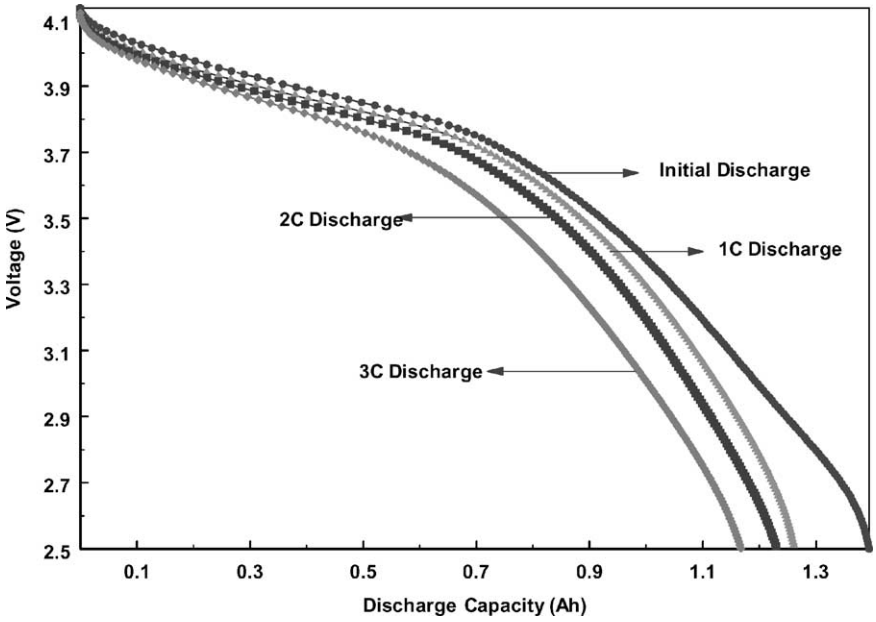

Fig. 3. Discharge voltage profile of fresh battery and batteries cycled up to 300 times under different discharge rates. The discharge current used was 0.7 A.

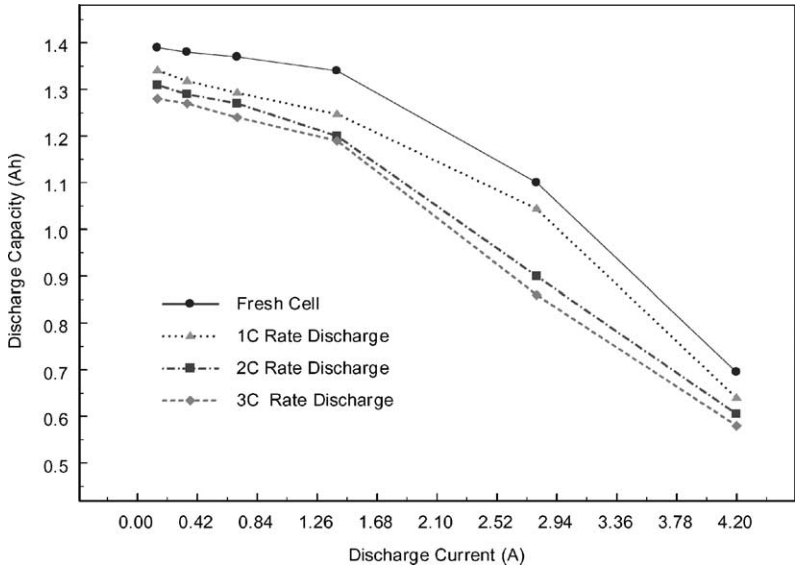

Fig. 4. Rate capability of fresh battery and batteries cycled up to 300 times under different discharge rates. Discharge rates used here represent 1/10, 1/4, 1/2, 1, 2 and 3*C*.

where E_0 is a state-of-charge-dependent equilibrium potential of the cell, I the discharge current and R_T is the total internal resistance of the cell including electrolyte resistance, resistance of cathodic and anodic polarization, contact resistance among particles of electrode materials and contact resistance between current collector and the electrode materials. It is clear that increasing the internal total resistance will definitely shorten the time for the cell to reach the cut-off voltage (2.5 V in our work). Discharge capacity is the product of the discharge current and discharge time, so shorter discharge times mean a lower discharge capacity (provided that the discharge current is the same). This indicates that the internal resistance of the whole battery cycled at a higher discharge rate is larger than that cycled at a lower discharge rate.

Fig. 4 presents rate capability studies on a fresh Sony US 18650 cell and cells cycled up to 300 times. All batteries were charged to the fully charged state with CC–CV protocol. They were then discharged to 2.5 V at different rates. The performance of all the cycled batteries was poor compared with the fresh battery. However, the batteries cycled at a higher discharge rate (3*C* discharge rate) showed the worst performance. This indicates that the performance of the battery has been hampered by the increase of the internal resistance.

Our next work focused on quantifying the increase of the internal resistance by measuring it as a function of depth of discharge (DOD). This was done by interrupting the discharge current by a 5-s rest pulse intermittently all through the process of discharge and recording the voltage change

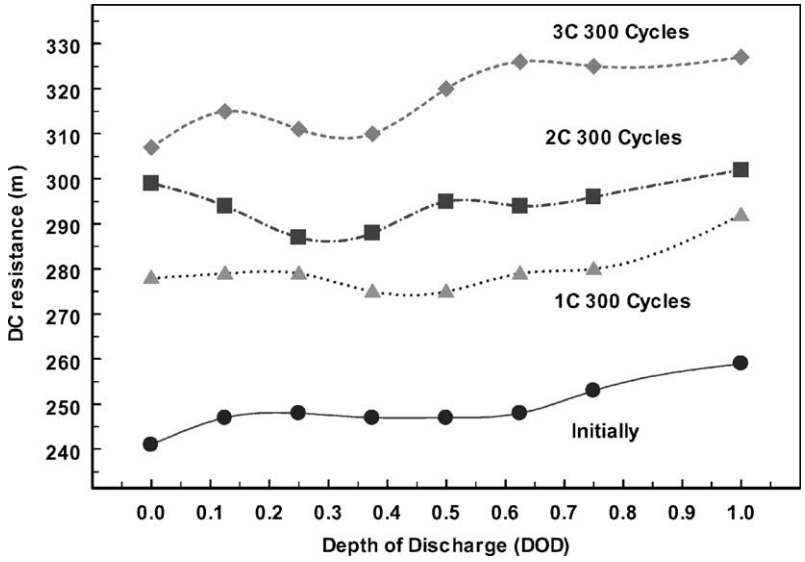

Fig. 5. dc resistance R_{dc} as a function of depth of discharge (DOD).

before and after interrupting the rest pulse. In our experiment, the computer was programmed to log the data 0.1 s after the pulse rest time, which was then used in a R_{dc} calculation. Fig. 5 presents the plot of R_{dc} as a function of DOD. In most cases, the internal resistance of the battery is around 200 mΩ, which is very similar to the results reported by the manufacturer. The R_{dc} corresponding to different DOD remained almost constant except that it increases slightly at the end of discharge. The largest deviation from the average resistance is not more than 3%. The internal resistance of the battery cycled at 1*C* discharge rate has increased by 12.4% while those cycled at 2*C* and 3*C* discharge rates show an internal resistance increase of 18.3 and 27.7%.

3.2. Charge and discharge study of half-cells

The capacities obtained from the half-cells under 150 μA charge and discharge rate was normalized based on the geometric area of the working electrode of the pellet ($\pi \times 0.55\,\text{cm} \times 0.55\,\text{cm}$), and then this value was multiplied by the total geometric area of the electrode area inside the commercial battery. Twice this value (because of double-side active material loading in this kind of cylinder battery) became the discharge capacity of the negative carbon electrode or positive $LiCoO_2$ electrode. Table 1 shows the capacity fade (in %) of the individual pellet electrodes as well as the calculated capacity fade (in %) of the whole lithium-ion battery after 300 cycles under 1*C*, 2*C* and 3*C* discharge rates. It is obvious that the capacity fade of the negative carbon electrode cycled under high rates contributes more to the fade of the whole battery. The total capacity fade of the whole-cell is not equal to the summation of the capacity fades of the positive electrode and the negative electrode. In the whole-cells, the mass ratio of positive electrode to negative electrode is designed according to the theoretical capacity of the active electrode materials themselves. On the basis of that ratio, an excess amount of $LiCoO_2$ was added to compensate for the loss of Li^+ to form surface film over the electrode surface (during the period of formation). Ideally after formation, the rest of the Li^+ should be able to shuttle back and forth between the positive and negative electrode without additional loss. But in reality, a small amount of Li^+ will be continuously consumed due to some unavoidable parasitic reactions (mainly continuing surface film formation reactions). Accordingly, the physical or chemical properties of the surface film will be altered with cycling. So the capacity loss of the whole battery should be directly related to the loss of lithium ions as well as individual electrode's ability to intercalate or deintercalate lithium ions. However, in the case of the half-cell studies, an excess amount of lithium salt and solvents were added to the T-cell, which means the capacity loss in this case is directly related to the loss of electrode material's ability to intercalate or deintercalate lithium ions. This could arise due to the change in the surface film or due to other causes whose change or whose effects can hamper the electrode's ability to intercalate or deintercalate. For convenience, we call this capacity loss due to the loss of secondary materials (which is named Q_2 later). And this can be measured directly from half-cell studies.

Table 1
Half-cell analysis of capacity fade (in %) of negative carbon electrode and positive $LiCoO_2$ electrode

Capacity fade	1*C* discharge rate (%; 300 cycles)	2*C* discharge rate (%; 300 cycles)	3*C* discharge rate (%; 300 cycles)
Carbon	2.77	8.30	10.59
$LiCoO_2$	3.98	4.38	5.18
Capacity fade of the whole cell (%)	9.50	13.20	16.90

The charge or discharge current used for the half-cell studies were 150 μA (approximately (*C*/20) rate) while the discharge current for the whole battery was 0.7 A ((*C*/2) rate).

Based on above analysis, the total capacity fade of the lithium-ion battery can be divided into three parts:

$$Q = Q_1 + Q_2 + Q_3 \tag{2}$$

where Q is total capacity fade of lithium-ion battery ($Q = C_0 - C_{300}$), where C represents the discharge capacity of the Li-ion battery at *C*/2 discharge rate while the subscripts 0 and 300 represent initial and after 300 cycles, respectively.

$Q_1$is the correction item due to different rate capability ($Q_1 = C_{C/2} - C_{C/20}$), where $C_{C/20}$ represents the capacity of the Li-ion battery at *C*/20 discharge rate while $C_{C/2}$ represents the discharge capacity of the same Li-ion battery at *C*/2 discharge rate.

Q_2 is capacity fade due to the loss of carbon electrode or $LiCoO_2$ electrode ($Q_2 = c_0 - c_{300} \times (2 \times (A_T/A_p))$), where the lower case c represents the capacity of half-cells, subscripts 0 and 300 represents the capacity initially and after 300 cycles, respectively. A_T represents the total geometric area of the electrode (the geometric area of positive $LiCoO_2$ electrode is 46.5 cm × 5.40 cm and that of negative carbon electrode is 47.5 cm × 5.6 cm), while A_p represents the geometric area of the punched pellet (equal to $3.1415 \times 0.55\,\text{cm} \times 0.55\,\text{cm}$). Q_2 could be due to either $LiCoO_2$ or carbon, the larger value of which is used in equation [2].

Q_3 is the capacity fade due to the loss of lithium ions and other reasons. It was indirectly calculated through charge balance.

If above Q, Q_1, Q_2, and Q_3 are divided by the initial capacity of the battery, above capacity fade will be expressed in the form of %.

$$Q' = Q_1' + Q_2' + Q_3' \tag{3}$$

It is found from Table 1 that the capacity fade of $LiCoO_2$ cycled to 300 times under 1*C* discharge rate (3.98%) outruns that of carbon (2.77%). This is similar to the result reported

Table 2
Breakdown of the total capacity fade of the whole lithium-ion battery

	1*C* discharge rate (%; 300 cycles)	2*C* discharge rate (%; 300 cycles)	3*C* discharge rate (%; 300 cycles)
Capacity fade of the whole cell (%)	9.5	13.2	16.9
Q_1'	3.5	2.9	2.8
Q_2' (due to carbon)	NA	8.4	10.6
Q_2' (due to $LiCoO_2$)	3.8	NA	NA
Q_3'	2.3	2.0	3.4

by Zhang et al. [6], whose conclusion is that the fast increase of the impedance of $LiCoO_2$ electrode is primarily due to the increase of the surface resistance due to oxidation process and that increase dominates the total resistance of the cell. In the case of the batteries cycled at 2*C* and 3*C* discharge rates, the capacity fade of carbon electrode becomes more, namely 8.4 and 10.6%, respectively. Increase in the impedance of both cathode and anode of Li-ion cells limit the discharge capacity of the cell or the cycle life of the cell, but the difference reflected in our experimental data is the fast capacity loss due to carbon when the battery was cycled under 2 or 3*C* discharge rates. It is shown from Table 2 that the Q_1 is very close in all the three cases, which is close to 3%. And Q_2 related to the loss of secondary material (carbon or $LiCoO_2$) is still the dominant reason for the total capacity fade of the whole lithium-ion battery, especially when the battery was cycled under high discharge rates. The following studies (EIS measurements) were aimed at explaining the loss of the ability to intercalate or deintercalate Li^+.

3.3. Electrochemical impedance spectroscopy (EIS) study

Fig. 6(a) and (b) show the Nyquist plots of a fresh whole-battery as well as of batteries cycled up to 300 times under different discharge rates. Unlike the dc resistance reported in earthier sections, the ac impedance is a strong function of state-of-charge. The impedance of the cell in the fully charged state is always lower than that in the fully discharged state. Also, the total impedance of the battery cycled at high discharge rates (2 or 3*C*) is larger than that of the battery cycled at a low discharge rate (1*C*) at both 0 and 100% SOC. The impedance spectra in the fully discharged state (0% SOC) clearly shows a few depressed semi-circles (the one at high frequencies is not as obvious as the other two for medium and low frequencies) with a straight sloping line indicating solid-state diffusion at low frequencies. In the spectra obtained in the fully charged state (100% SOC), it is hard to differentiate separate semi-circles. To understand the contribution of individual electrodes to the performance of the full cell, EIS studies on half-cells were done in order to clarify the individual capacity fades of negative and positive electrodes.

Prior to EIS measurements, the assembled half-cell had been fully charged and fully discharged at 75 μA. The charge/discharge time between the fully discharged state and the fully charged state of the half-cell in the first cycle has been used as the reference for the calculation of the state-of-charge or depth of discharge. Suppose the charge time for the half-cell is *T* in the first cycle, the SOC is determined by (τ/T), where τ denotes the charge time before the EIS measurement. DOD is calculated the same way. For $LiCoO_2$ half-cells, high SOC corresponds to high potential of the half cell while for carbon half-cells high DOD is correlated to high potential of the half cell. No appreciable capacity fade of the half-cell was found in the first 4–5 cycles.

Numerous papers have been published with regard to the interpretation of the EIS spectra as well as version models to fit the spectra [1,2,7,8]. A modified version of the Voigt–FMG model that is basically a combination of a Voigt-type analog and the generalized Frumkin and Melik-Gaykazyan impedance was used to interpret the lithium intercalation into graphite [2]. The shortcoming with this model is that it does not take into account the electronic resistance of the bulk electrode materials. Based on the shape of the observed spectra and results previously used by other groups [1,2,5,7–10], we decided to utilize Croce's model [5,12] to analyze our EIS spectra. In this model, the high frequency depressed semi-circle is interpreted as the migration of Li^+ through the multi-layered surface films (solid electrolyte interface, SEI). The middle frequency semi-circle is related to the charge-transfer resistance across the interface and the low frequency semi-circle is associated with the electric conductivity (or resistance) of the bulk electrode material. At low frequencies, the sloping line (typical characteristics of Warburg diffusion region) accounts for the solid-state diffusion of Li^+ in the bulk electrode material. Although this model and interpretation was helpful in our analysis, there should be other models that can similarly interpret this complicated system. Fig. 7 is the equivalent circuit constructed based on the above interpretation of the spectra of EIS.

In the equivalent circuit, R_{elect} represents the resistance of Li^+ conduction in the liquid electrolyte while the three RC parallel elements in series are related to the passivating surface layer, charge-transfer and electronic resistance of the material, respectively. In subsequent data fitting, *Q* (constant phase element) instead of capacitance has been used to offset the depression of the semi-circle. Apart from those elements, the circuit also takes into account Warburg diffusion impedance (Z_w) and the intercalation capacitance (C_{int}) that can be observed only at extremely low frequency. Considering the limited size of the particles, we adopted the finite-length Warburg-type element Z_w [11]. C_{int}, the intercalation capacitance, simulates the accumulation and consumption process of Li^+ in the bulk material. Based on this model, at the lowest frequency, the EIS spectra measured from these electrodes should be able to reflect the capacitive behavior of the bulk intercalation of the electrode materials with the characteristic of an almost vertical line in the lowest frequency region in Nyquist plots. But such a region does not appear in our impedance spectra. It is because the lowest

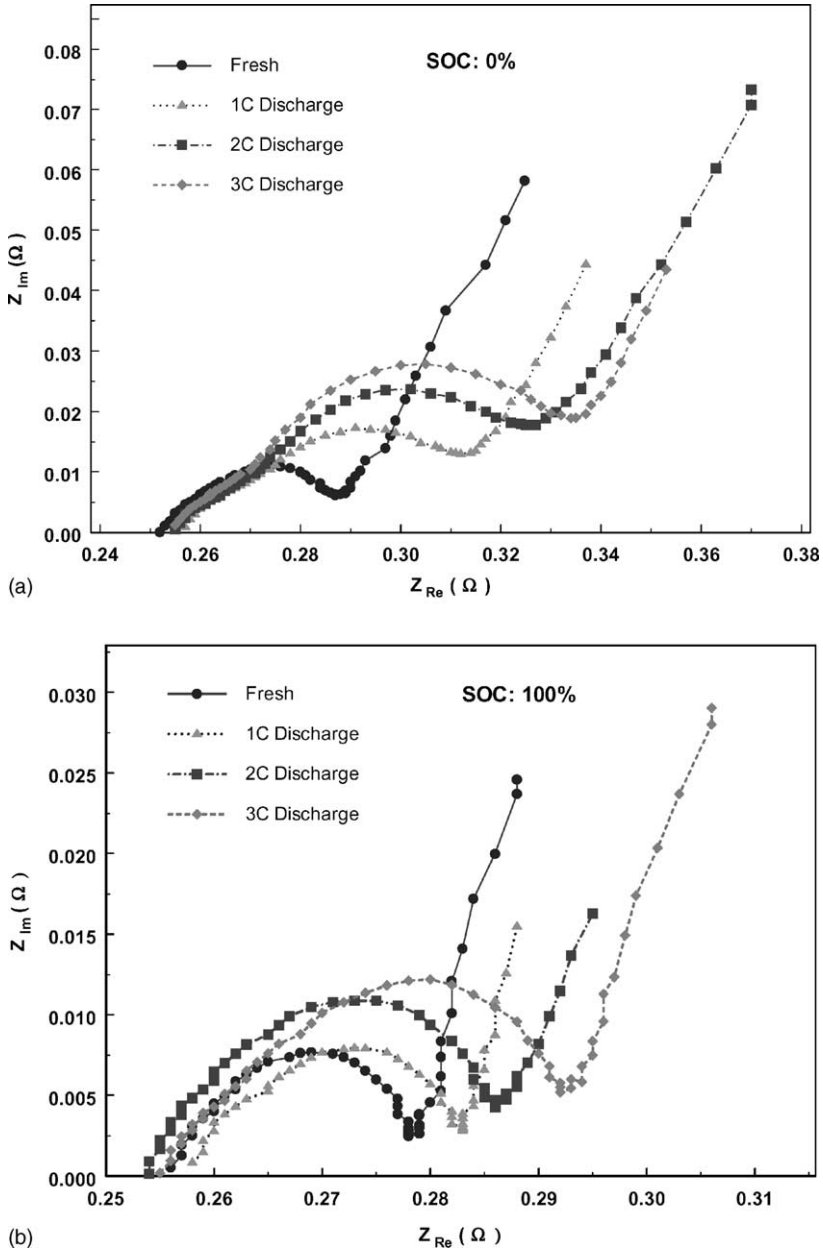

Fig. 6. Nyquist plots of fresh battery and batteries cycled up to 300 cycles under 1, 2, 3*C* discharge rates (a) 0% SOC; (b) 100% SOC. The geometric area of the $LiCoO_2$ positive electrode in the Li-ion battery is 46.5 cm × 5.4 cm and the geometric area of carbon negative electrode is 47.5 cm × 5.6 cm.

frequency (1 mHz) we applied (due to our experimental limit) is not sufficiently low enough to reach that theoretical region. However, C_{int} can be obtained through fitting the model in Fig. 7 with the experimental data.

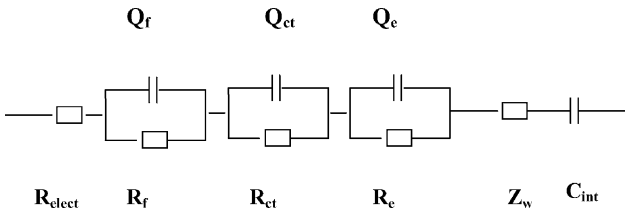

Fig. 7. Equivalent circuit of the EIS spectra.

To ensure the accuracy of data fitting for comparison among properties of different-discharge-rate-cycled materials, we only chose the data corresponding to 10 and 20% DOD. Fig. 8 shows the results. As can be seen, the resistance of the surface film (R_f) is in the range from 2 to 10 Ω. These results are consistent with those published by Croce and Scrosati [5]. Under both 10 and 20% DOD, R_f increases with the increase of discharge rate used in battery cycling. This shows it is likely that products of parasitic reactions deposit on the surface of the carbon material at a faster rate when the battery was cycled under a higher discharge rate. As a result, the total thickness of the surface film increases quickly. The electronic resistance of the bulk material (R_e) similarly

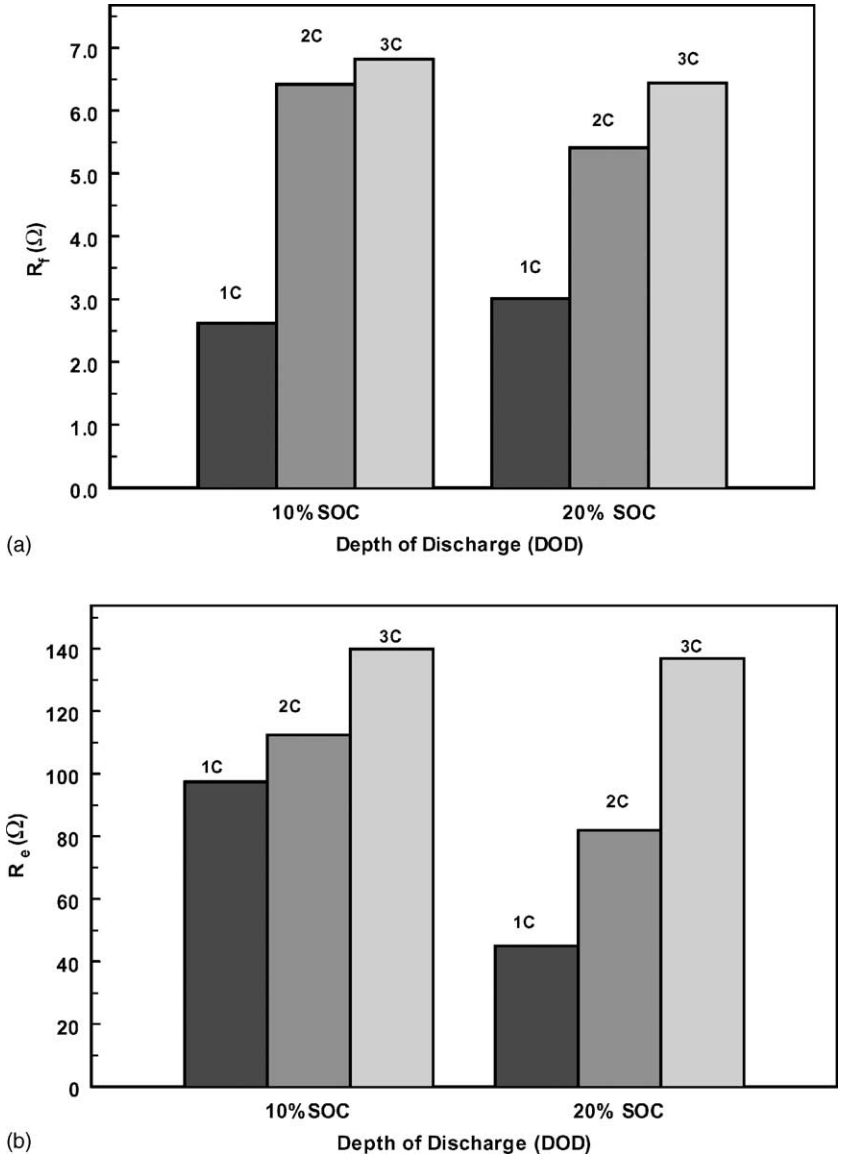

Fig. 8. Comparisons of parameters (a) R_f resistance of surface film; (b) R_e electronic resistance of the bulk carbon material. Above data were obtained through fitting the model in Fig. 7 with the experimental spectra of EIS of carbon half-cells (with carbon material cycled at 1, 2, and 3*C* discharge rate).

follows the trend of the resistance of the surface film (R_f). Since the semicircles in the middle-range frequencies are not clearly defined, we did not use R_{ct} values obtained through this fitting method for comparison. As far as the magnitude is concerned, the electronic resistance of the bulk material dominates the total impedance of the carbon half-cell.

The other very important parameter we have indirectly obtained is the ionic chemical diffusion coefficient in the solid-phase carbon materials [2,3,13]. Based on a SEM study, the average diffusion length l was supposed to be equal to the size of the particle, which is 5 μm for the carbon material. The chemical diffusion coefficient was calculated from C_{int} values that were obtained through fitting experimental data with the model. The value is approximately of the order of 10^{-10} cm^2/s and it changed little after 300 cycles.

Obviously, the increase in the resistance of the surface film (R_f) as well as of the electronic resistance (R_e) resulted in fast capacity fade of the carbon half-cell. This also led to an increase in capacity fade of the whole Li-ion cell cycled at higher discharge rates. One plausible explanation of the fast increase of those physical properties of carbon with cycling is that the surface film formed on the carbon electrode may not be as firm or protective as it is expected to be, especially when the battery is cycled at a high discharge rate. Continuous small-scale electrolyte or salt reduction on the carbon electrode surface is inevitable due to the instability of the electrolyte towards the carbon under cathodic conditions, especially when the surface film formed during early formation is neither fully formed nor solid on the surface of the electrode material [1]. It is known that those reactions will take place when the potential of the carbon electrode is below 1.5 V versus Li^+/Li.

The overall electrochemical decomposition of solvents in the battery such as EC or DMC can be expressed as [14]

$$2Li^+ + 2e^- + 2(CH_2O)CO\,(EC) \rightarrow CH_2(OCO_2Li)CH_2OCO_2Li\downarrow + CH_2CH_2 \quad (4)$$

$$2Li^+ + 2e^- + (CH_2O)CO\,(EC) \rightarrow Li_2CO_3\downarrow + C_2H_4\uparrow \quad (5)$$

$$Li^+ + e^- + CH_3OCH_2CH_3\,(DMC) \rightarrow CH_3OCO_2Li\downarrow + CH_3 \quad (6)$$

The reduction products are the primary components of the thickened SEI film on the carbon electrode. It also can be seen from above reaction formulae that gaseous products will be formed at the same time. In parallel with those side reactions, the solvent can co-intercalate into the carbon structure to form a ternary graphite intercalation compounds (GIC), and is a direct cause of the exfoliation of the carbon and the expansion of the carbon particles.

For the batteries cycled at high discharge rates, the internal temperature was high. Ohm's law can easily explain this phenomenon. The heat generated during discharge can be given by: $w = I^2 \times R$ [7].

More heat is generated per unit time and accordingly the internal pressure during cycling should be higher with a high discharge rate. However, the internal temperature could not be easily measured during the cycling because it is almost impossible to put a thermal couple into the battery without causing damage to the battery. Randolph et al. [15] reported that the difference between the internal and external temperature of an overcharging cell could be as high as 60 °C under a high current discharge. The heat generated will not easily dissipate from the battery to the outside environment. The reduction reaction on the surface of carbon electrode will proceed at a faster rate due to high internal temperature and more and more gas will be formed in a short period of time. The buildup of pressure due to those gaseous products and the evaporation of the electrolytes at high temperature during cycling might easily stretch or damage the surface film. As a consequence, Li^+ and electrolyte will go through enlarged cracks or newly formed cracks and react with the internal lithiated carbon particles. Actually we found more cracks as

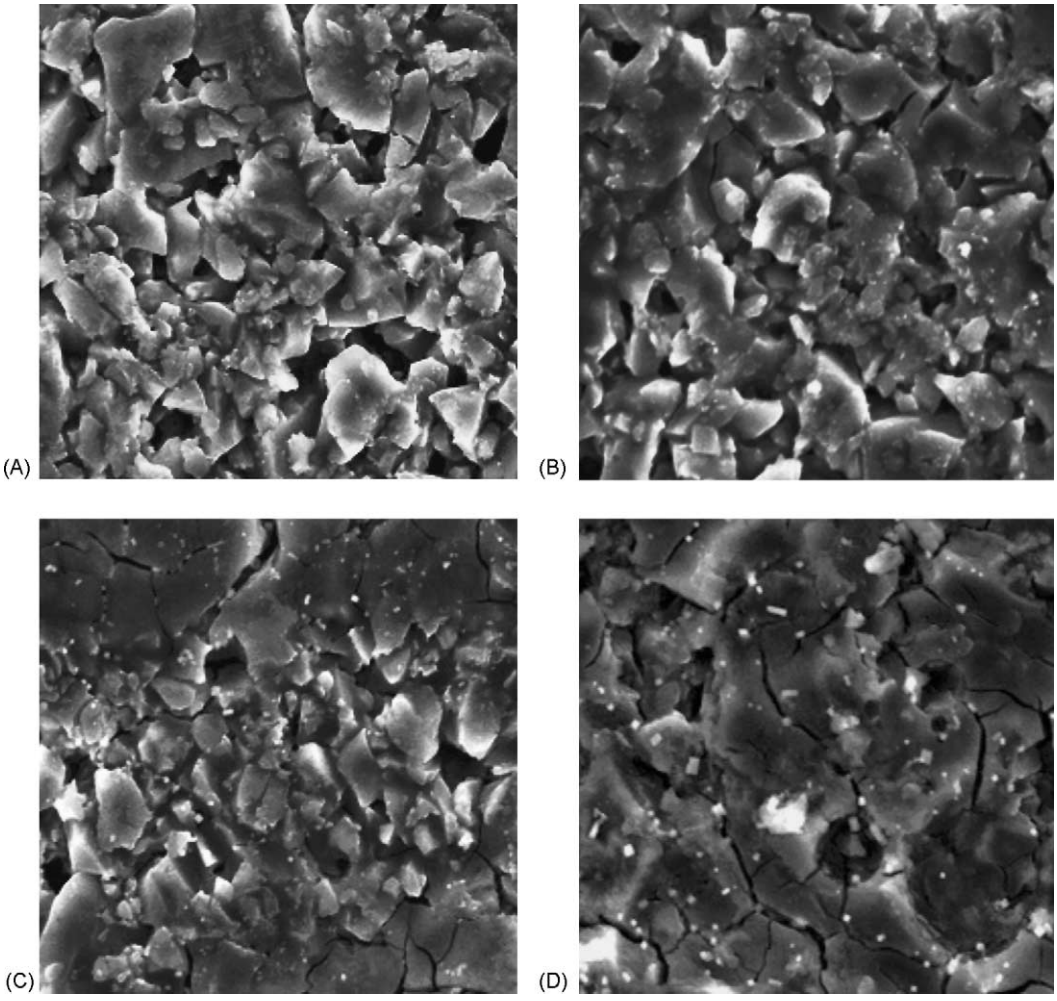

Fig. 9. SEM (1000×) of carbon materials cycled at different discharge rates. (A) Carbon cycled at 1*C*; (B) carbon cycled at 2*C* discharge rate; (C) and (D) carbon cycled at 3*C* discharge rate.

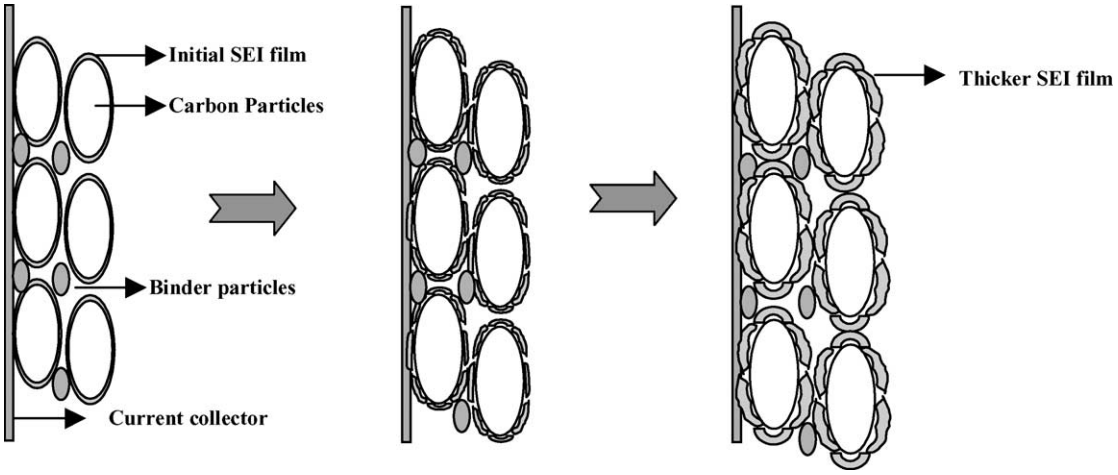

Fig. 10. Evolution of the SEI film on the surface of carbon when the battery is cycled.

well as some white color substances (lithium salts) on the surface of the carbon electrode when we cut open the battery to take out the electrode materials. Fig. 9 shows SEM images of carbon samples cycled at 1*C*, 2*C* and 3*C* discharge rates. It can be seen in Fig. 9A (1*C*-discharge-rate-cycled carbon) that the surface of the carbon electrode is smooth and clean, however some white substances are dispersed on the surface in Fig. 9B (2*C*-discharge-rate-cycled carbon). When it comes to the carbon samples of 3*C* in Fig. 9C and D, we see not only more white substance but also more cracks on the surface. Based on the impedance analyses and the morphology of the surface of the materials, we believe that the reactions between the organic solvents or Li^+ and lithiated carbon have never completely stopped because the active species can easily percolate the crevices on the film and reach the lithiated carbon. The products of those side reactions provide enough material for the formation of a new SEI film. So with cycling, the surface film becomes thicker and thicker. Fig. 10 is a schematic of this surface thickening process.

When the battery is cycled under a high discharge rate, the internal temperature will rise quickly and the surface film on the carbon particles becomes thicker quickly, so it is easy to understand the increase of R_f which is physically correlated with the migration of Li^+ through the SEI film.

4. Conclusion

A systematic capacity fade study was done for Sony US 18650 batteries cycled at normal and high discharge rates. Three major causes of capacity fade including the loss of secondary material, the loss of primary material and the difference of rate capability were quantified. In each case the loss of the secondary material dominated the capacity fade of the whole cell. However, unlike the 1*C*-discharge-rate-cycled battery, the limiting secondary material the in 3*C*-discharge-rate-cycled cell was carbon. The capacity loss due to the carbon electrode material alone was 10.6% compared with the 16.9% capacity fade of the whole cell. Such a fast capacity fade for the carbon material is correlated with the increase of the internal resistance. Fitting impedance spectra for the carbon half-cell quantitatively showed that the resistance of the surface film and the resistance of the bulk carbon material increase faster for high-rate-discharged cells than for normal-rate-discharged cells. SEM images further demonstrate more material deposited on the surface of the high-discharge-rate-cycled carbon. One cause for the parasitic reactions to continue is the protective SEI film cracks due to high temperature which results from high rate discharging.

Acknowledgements

The authors are grateful for the financial support provided by the National Reconnaissance Organization (NRO) under Contract No. NRO-00C-0134.

References

[1] P. Arora, R.E. White, M. Doyle, J. Electrochem. Soc. 145 (1998) 3647.
[2] M.D. Levi, D. Aurbach, J. Electrochem. Soc. 146 (1999) 1279.
[3] M.D. Levi, D. Aurbach, Electrochim. Acta 45 (1999) 167.
[4] K. Ozawa, S.S. Ionics 69 (1999) 212.
[5] F. Croce, B. Scrosati, J. Phys. Chem. B 106 (2002) 3909.
[6] D. Zhang, B.S. Haran, A. Durairajan, R.E. White, B.N. Popov, J. Power Source 91 (2000) 122–129.
[7] A. Funabiki, M. Inaba, Z. Ogumi, J. Power Source 68 (1997) 227.
[8] C. Wang, A.J. Appleby, F.E. Little, Electrochim. Acta 46 (2001) 1793.
[9] F. Croce, F. Nobili, Electrochem. Commun. 1 (1999) 605.
[10] F. Varsano, F. Croce, Electrochim. Acta 46 (2001) 2069.
[11] J.R. Macdonald, Impedance Spectroscopy, Wiley, New York, 1987, p. 60.
[12] P.G. Bruce, M.Y. Saidi, J. Electroanal. Chem. 322 (1992) 93.
[13] C. Ho, I.D. Raistrick, R.A. Huggins, J. Electrochem. Soc. 127 (1980) 343.
[14] A.M. Anderson, K. Edstrom, Electrochim. Acta 47 (2002) 1885.
[15] R.A. Leising, M.J. Palazzo, E.S. Takeuchi, K.J. Takeuchi, J. Electrochem. Soc. 148 (2001) A838.